

Learning Cross-Scale Prediction for Efficient Neural Video Compression

Zongyu Guo^{1*} Runsen Feng^{1*} Zhizheng Zhang² Xin Jin¹ Zhibo Chen^{1†}

¹University of Science and Technology of China

²Microsoft Research Asia

{guozy, fengruns, jinxustc}@mail.ustc.edu.cn, zhizzhang@microsoft.com, chenzhibo@ustc.edu.cn

Abstract

In this paper, we present the first neural video codec that can compete with the latest coding standard H.266/VVC in terms of sRGB PSNR on UVG dataset for the low-latency mode. Existing neural hybrid video coding approaches rely on optical flow or Gaussian-scale flow for prediction, which cannot support fine-grained adaptation to diverse motion content. Towards more content-adaptive prediction, we propose a novel cross-scale prediction module that achieves more effective motion compensation. Specifically, on the one hand, we produce a reference feature pyramid as prediction sources, then transmit cross-scale flows that leverage the feature scale to control the precision of prediction. On the other hand, we introduce the mechanism of weighted prediction into the scenario of prediction with a single reference frame, where cross-scale weight maps are transmitted to synthesize a fine prediction result. In addition to the cross-scale prediction module, we further propose a multi-stage quantization strategy, which improves the rate-distortion performance with no extra computational penalty during inference. We show the encouraging performance of our efficient neural video codec (ENVC) on several common benchmark datasets and analyze in detail the effectiveness of every important component.

1. Introduction

The ML-based methods have shown promise in reshaping the field of data compression. The success in neural image compression [6, 11, 18, 38, ...] clearly demonstrates the coding efficiency of ML-based methods. But video compression is a more challenging task, due to the complicated inter frame redundancies. The evolutionary history of traditional video coding standards [9, 43, 47, ...] proves the significance of inter frame prediction. A good prediction module should be

aware of the content variety of video frames and be adaptive to various motion cases.

Many neural video codecs have been designed in the past few years. Some are proposed for the low delay setting, reducing the temporal redundancies by unidirectional prediction [2, 10, 21, 23, 28, 31, 32, 35, 42]. Some can be used for the random access setting, making use of bidirectional references to predict the target frame [15, 41, 48, 50]. In this paper, we focus on the simplest low-latency mode, *i.e.*, always predicting the target frame with the previous single reconstructed frame. This is the most basic scenario of inter frame prediction, which reveals the ability of a video codec in exploiting the temporal redundancies within two consecutive frames. Actually, a successful neural video codec designed for this scenario (single-reference prediction) can easily be extended to other prediction scenarios [28, 41].

DVC [35] is a typical method designed for this scenario. DVC follows the classical hybrid coding framework [20], compressing the 2-D motion vectors as optical flow and then compressing the pixel residuals by end-to-end optimization. The optical flow describes the motion displacement of every pixel, utilized to generate the warping result (the predicted frame). However, prediction with 2-D optical flow fails frequently when the motion is fast or where there is no reference for frame prediction, such as disocclusion. To this end, the later work SSF [2] applies multi-level Gaussian smoothing on the reference frame and performs trilinear warping in Gaussian-scale space [30]. The scale dimension in SSF allows the model to blur the source content before prediction, reducing the errors caused by the direct warping of optical flow. But Gaussian smoothing is computed with stationary blurring pattern, not fully adaptive to diverse video content. Recently, FVC [23] suggests learning reference representations for feature-level prediction, which also reduces prediction artifacts of pixel-level warping. However, regarding the learned reference sources, there is no concept of scale to explicitly control the prediction precision. Such feature-level prediction thereby cannot adapt to video

*Equal contribution.

†Corresponding author.

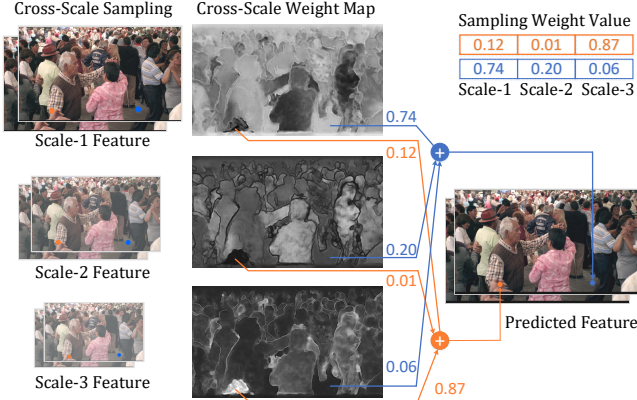


Figure 1. The proposed cross-scale prediction. Our model generates prediction sources at three scales. Cross-scale flows are transmitted to determine the sampling locations across scales. Corresponding weight maps describe the importance of sampling results.

content and fails to handle various motion cases.

In this paper, towards fine-grained content-adaptive prediction, we propose a novel cross-scale prediction module, achieving much more effective motion compensation in the scenario of single-reference prediction. While processing features at multiple scales is one of the most successful techniques for computer vision [29, 33, 53], we show that in the task of neural video compression, we can produce a reference feature pyramid for flexible prediction in various motion cases. The high-resolution reference features are well-suited for prediction in the case of simple motion, *e.g.*, translational motion, since the high-resolution features preserve most of the context and deliver a high-precision prediction. Meanwhile, we can generate the low-resolution reference features with strong semantic information, to further reduce the prediction error in the cases of fast motion or disocclusions. After producing the reference feature pyramid, our model will transmit cross-scale flows as a set of displacement vectors that attend to the multi-scale prediction sources. Therefore, our neural video codec can cover multiple prediction precisions.

While producing a reference feature pyramid provides more options on prediction sources, it is still hard to support fine-grained adaptation to diverse motion content. Motivated by previous works that apply weight maps for prediction with multiple reference frames [15, 25], we introduce the mechanism of weighted prediction to compute a content-adaptive prediction result even in the scenario of single-reference prediction. Specifically, we transmit cross-scale weight maps as a part of motion information to describe the importance of each sampling result. We highlight that the reference features learned at multiple scales are complementary to each other in various motion cases. As shown in Figure 1, the region with simple motion will pay more attention to high-resolution prediction result (assign larger weight value to scale-1, the

blue point). The region with fast motion (the orange point) will be predicted with larger weight value assigned to the low-resolution scale (scale-3 in Figure 1). Therefore, our proposed cross-scale prediction module can adapt to diverse motion content and synthesize a fine prediction result.

In addition, we also propose a multi-stage quantization strategy that only affects the training process of our neural video codec but delivers higher coding efficiency during testing. Such multi-stage quantization strategy helps to close the train-test mismatch, which is an underlying issue of additive uniform noise-based quantization [5]. We term this strategy as the video-version soft-then-hard, as it is improved from the image-version soft-then-hard [19].

In short, our contributions are summarized as follows:

- We propose cross-scale prediction with a single reference frame, supporting fine-grained adaptation to diverse motion cases, as our core contribution.
- We propose a multi-stage quantization strategy, improving the RD performance of neural video codec with no extra computational penalty during inference.
- We carefully build our neural video codec and achieve the encouraging rate-distortion performance.

While most previous neural video codecs can barely compete with H.265/HEVC, our proposed efficient neural video codec (ENVC) can compete with H.266/VVC [9] in terms of sRGB PSNR under the same prediction configuration (single-reference prediction) on UVG dataset [39]. When optimized for the MS-SSIM metric [46], ENVC outperforms VVC obviously. We also show our encouraging performance on other common benchmark datasets, including HEVC test sequences [43] and MCL-JCV [45]. We further conduct a comprehensive study to analyze every important component that contributes to our state-of-the-art performance.

2. Related Work

2.1. Lossy Image Compression

Despite a short history, neural image codecs have outperformed the latest image compression standard H.266/VVC intra regarding sRGB PSNR [18] and MS-SSIM [11]. Currently, most prevailing neural image codecs follow the VAE framework [5, 6]. A series of works are built upon this framework, improving from the aspects of entropy estimation [11, 18, 26, 40], quantization [1, 3, 5, 19, 51], variable rate [12, 13] and perceptual quality [4, 38]. Among them, we note that the autoregressive context model [26, 40] can achieve obvious rate savings but bring much more decoding complexity. In this paper, we build two versions of video codecs, with or without the autoregressive (AR) model. The former achieves the best rate-distortion (RD) performance while the latter is more applicable in practice.

2.2. Video Compression

It takes decades to develop a new generation of video coding standard. The classical standards H.264/AVC [47] and H.265/HEVC [43] are in broad use, and the recent standardized H.266/VVC [9] will soon be applied in industry. All of these standards follow the hybrid coding framework, developed with handcrafted modes. Technically, in a video codec, the intra frame coding is equivalent to image coding. And the challenge for video compression mainly exists in efficient compression of inter frames.

Neural video compression approaches are on the way catching up with traditional standards. Existing works in this field can be classified into two categories, designed for low delay setting [2, 10, 21, 23, 28, 31, 32, 35, 42] and random access setting [15, 41, 48, 50]. The low delay setting is suitable for applications such as live streaming, which only uses the past frame(s) to predict the current frame. For the random access setting, the reference frame can be from future, well-suited for applications such as playback. In addition, there are works designing a unified model for both settings [16, 25].

The compression model applied for the low delay setting is termed as a P-frame model. Many techniques have been proposed to improve the coding efficiency of P-frame model, such as 3D autoencoders [21], conditional entropy coding [21, 27, 32], online updating [34] and effective prediction in hybrid coding. For these hybrid coding solutions, they further involve two prediction modes, *i.e.*, prediction with single or multiple reference frames. The aforementioned DVC [35], SSF [2] and FVC [23] are typical works improving single-reference prediction. Some multi-frame fusion modules are also designed for unidirectional prediction with multiple reference frames [23, 28, 42]. Obviously, fusing more reference frames benefits the RD performance, but also brings a significant increase of memory cost.

A successful P-frame model designed for single-reference prediction can easily be extended to unidirectional multiple-reference prediction or bidirectional prediction. Therefore, prediction only with the previous frame is the most basic case for video compression, as the main concern of our paper.

3. Method

3.1. Overview

An overview of our P-frame compression model is shown in Figure 2, which follows a typical hybrid coding framework [20]. Our P-frame model mainly contains a motion compression network and a residual compression network, both are in the style of autoencoders [5]. Here, we introduce them respectively by describing the scale (spatial resolution) of some important inputs and outputs inside the framework. The detailed network structures for down/up-sampling and encoding/decoding will be described later in Section 3.3.

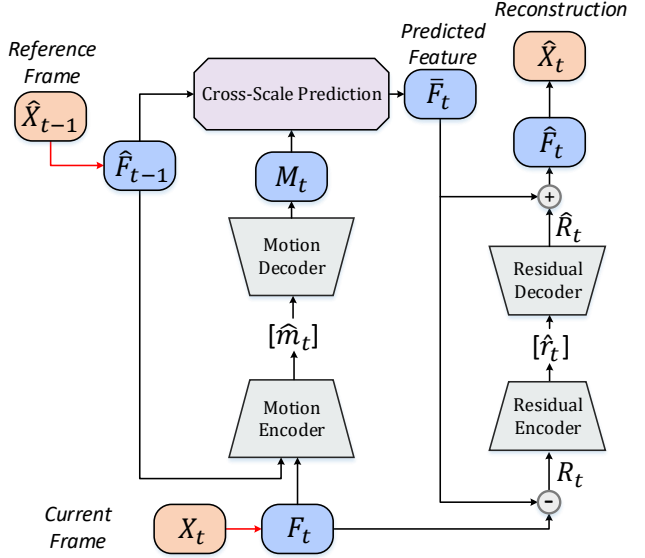


Figure 2. An overview of our P-frame compression model, applied for the low latency mode with single-reference prediction. All blue features are at the scale of $1/2$ original resolution.

Motion Compression. Given the reference frame \hat{X}_{t-1} , which is the lossy reconstruction of the previous frame, it will first be transformed into reference feature \hat{F}_{t-1} by a feature extractor (denoted by the red arrow in Figure 2). The current frame X_t will also be transformed into feature F_t , using the same feature extractor. Assume the spatial resolution of X_t is $H \times W$, then both \hat{F}_{t-1} and F_t are features at scale $\frac{H}{2} \times \frac{W}{2}$. \hat{F}_{t-1} and F_t will be concatenated and sent into a motion encoder, generating the quantized variables \hat{m}_t at scale $\frac{H}{16} \times \frac{W}{16}$. On the decoder side, the motion decoder will upsample \hat{m}_t for three times, outputting M_t with scale $\frac{H}{2} \times \frac{W}{2}$. Here, M_t refers to the received motion information, which will participate in cross-scale prediction with the original reference feature \hat{F}_{t-1} . The mechanism of this prediction module will be introduced later in Section 3.2.

Residual Compression. The result of cross-scale prediction is the predicted feature \bar{F}_t at scale $\frac{H}{2} \times \frac{W}{2}$. We then compute the feature-level residual [17] as

$$R_t = F_t - \bar{F}_t. \quad (1)$$

The feature residual R_t will be downsampled in a residual encoder and is then quantized into latent variables \hat{r}_t . A residual decoder will decode out \hat{R}_t at the scale of $\frac{H}{2} \times \frac{W}{2}$. Now we can reconstruct the target feature \hat{F}_t :

$$\hat{F}_t = \bar{F}_t + \hat{R}_t. \quad (2)$$

Finally, a simple upsampling module will transform \hat{F}_t into \hat{X}_t , as the final reconstructed frame.

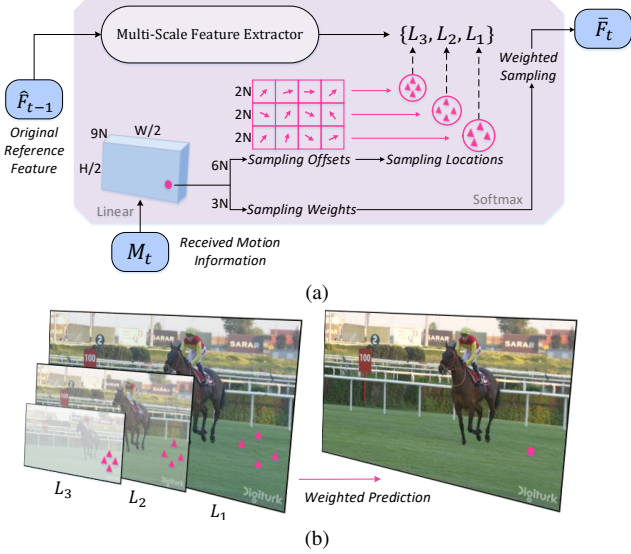


Figure 3. (a) Our proposed cross-scale prediction module. (b) Weighted prediction by aggregating cross-scale sampling results.

3.2. Cross-Scale Prediction

Here, we introduce the novel cross-scale prediction module in detail. In Figure 2, we can see the inputs of this module include the original reference feature \hat{F}_{t-1} and the received motion information M_t . The output is the predicted feature \bar{F}_t . All of them are at the scale of $\frac{H}{2} \times \frac{W}{2}$. However, inside the prediction module, features are processed at three scales.

As shown in Figure 3a, the original reference feature \hat{F}_{t-1} will be sent into a multi-scale feature extractor to generate a reference feature pyramid $\{L_3, L_2, L_1\}$. The scales of L_3, L_2, L_1 are $\frac{H}{8} \times \frac{W}{8}$, $\frac{H}{4} \times \frac{W}{4}$ and $\frac{H}{2} \times \frac{W}{2}$. The received motion information M_t will pass through a linear projection layer to generate sampling information. Every sample is described with a 3-channel vector, including the horizontal and vertical displacement, and a corresponding weight value. At each scale, the reference feature is sampled for N times. Since we have three scales in total, there are $(3N)$ sampling results for every target spatial location. And the sampling information should be a tensor with size $(9N) \times \frac{H}{2} \times \frac{W}{2}$, including $(6N) \times \frac{H}{2} \times \frac{W}{2}$ as the sampling offsets (named *cross-scale flows*) and $(3N) \times \frac{H}{2} \times \frac{W}{2}$ as the sampling weights. All the $(3N)$ sampling results are aggregated according to the softmax-computed sampling weights (named *cross-scale weight maps*). Figure 3b illustrates the aggregation process when N is 4, as our final setting.

The above introduction is a simplified version of our model. Inspired by [53], we further apply multi-head warping, where we first project the reference feature pyramid into four channel groups. In each channel group, our model repeats the same operation of cross-scale prediction. As a result, we will obtain multiple groups of predicted features,

which are then integrated by another linear projection layer. The visualization in Figure 3 can be regarded as the case when head number is 1. We set head number as 4 in our final model, which is found to accelerate the convergence during training. That is to say, the actual sampling information is described as a tensor with shape $(9N \times 4) \times \frac{H}{2} \times \frac{W}{2}$.

Discussion 1. Our proposed prediction module is *cross-scale* due to two reasons. First, the prediction sources come from a multi-scale feature pyramid but the prediction result is at the single scale of $\frac{H}{2} \times \frac{W}{2}$. That is to say, the cross-scale prediction module itself can aggregate information from multi-scale reference features, without the help of a down-to-top FPN structure [29]. Second, corresponding weight maps are also transmitted to describe the importance of multi-scale reference features. The weight map plays an important role for fine-grained adaptation to various motion cases, and forms a new mechanism for single-reference prediction, *i.e.*, weighted prediction.

Discussion 2. We also want to discuss the differences between our method and some previous methods. Our method is much more effective than the multi-scale prediction in NVC [31], because NVC pursues accurate prediction at all scales, going against our motivation, *i.e.*, complementary prediction across scales. Besides, we adopt multi-head warping, similar to the channel grouping operation in [23]. But we apply a linear projection layer to group the reference features. The transmitted cross-scale flows are analogous to the offsets of deformable convolution [14, 52], especially multi-scale deformable convolution [53]. We leverage them as motion descriptors for fine-grained prediction in the task of neural video compression.

3.3. Detailed Network Structures

In Section 3.1 and 3.2, we introduce our P-frame compression model by describing the scales of some important features. Here we add some details about the network structures. Each down/up-sampling layer is enhanced by three resblocks, the same as [17, 23, 31]. There are three autoencoders in our video codec, one for I-frame compression, one for motion compression and one for residual compression. Each autoencoder is enhanced by resblocks as well. The feature extractor ($X_t \rightarrow F_t$) and the final upsampling module ($\hat{F}_t \rightarrow \hat{X}_t$) consist of one down/up-sampling layer with resblocks. To compute the feature-level residual [17], the current feature F_t and the predicted feature \bar{F}_t are aligned by resblocks before generating the residual R_t . More specific details are provided in Appendix A, including the structures of the residual block and the entropy model.

3.4. Training and Quantization Strategy

Training an entire neural video codec is a systematical task. End-to-end optimization is the superiority of neural

video compression, but also results in some other issues. Here, we first introduce our training strategy in detail and then propose a multi-stage quantization strategy.

Training Strategy

Our neural video codec contains an I-frame model and a P-frame model, both of which are pre-trained in advance. To shorten the period of the initial training of the P-frame model, the target frame is first predicted with lossless reference frame. After pretraining, the I-frame and P-frame models are optimized jointly with the average rate-distortion loss. Specifically, if the training GoP size is T , then the total loss for joint training at this stage can be formulated as

$$\begin{aligned} \mathcal{L} &= \mathcal{R} + \lambda \cdot \mathcal{D} \\ &= \mathcal{R}_I + \lambda \cdot \mathcal{D}_I + \sum_{t=1}^{T-1} (\mathcal{R}_t + \lambda \cdot \mathcal{D}_t). \end{aligned} \quad (3)$$

Here, \mathcal{R}_I - \mathcal{D}_I and \mathcal{R}_t - \mathcal{D}_t represent the rate-distortion of the I-frame and the t -th P-frame. Since now the new P-frame is predicted by the previous lossy reconstructed frame, the reconstruction error will accumulate, which is known as the issue of temporal error propagation. To mitigate this issue, we could train with video sequences as long as what we evaluate on. However, this is infeasible in practice due to the huge GPU-memory cost. Therefore, the joint training is further divided into two stages. We first perform joint optimization with $T = 3$ and then increase T to 5 to finetune the entire model.

Soft-then-Hard Quantization for Training Video Codec

Since the gradient of quantization is zero almost everywhere, it makes the standard back-propagation inapplicable. A popular solution is to apply additive uniform noise (AUN) to approximate rounding during training [5], which will lead to the train-test mismatch issue [3, 19]. The work of [19] proposes a simple yet effective soft-then-hard (STH) strategy for training image compression models, which first optimizes with AUN and then conducts ex-post tuning. At the tuning stage, the analysis encoder g_a and the hyper encoder h_a are fixed. Meanwhile, the synthesis decoder g_s and the entropy decoder h_s are tuned with the hard-quantized variables. As a result, the decoder and the entropy model can be optimized by minimizing the true rate-distortion value. Unlike straight-through estimator (STE) [7] that cannot be used for entropy estimation, STH can close the train-test mismatch in both the synthesis decoder and entropy decoder.

For video compression, since the P-frame compression model is recurrently used, the reconstruction of the previous P-frame will affect the quantized latent variables of the next P-frame. Therefore, the soft-then-hard strategy [19] designed for image codec cannot be directly applied here. We propose to gradually close the train-test mismatch of additive uniform noise, as the video-version soft-then-hard, which

Training Stage	Fixed Components	Quantization Settings
① I-frame pre-training	None	AUN
② P-frame pre-training	None	AUN
③ Joint training (T=3)	None	AUN
④ Joint training (T=5) (+ modulated loss)	None	AUN
⑤ Joint training (T=5) (I-frame STH)	I-frame g_a and h_a	Hard for I-frame g_s, h_s AUN for P-frame model
⑥ Joint training (T=5) (P-frame STH)	Entire I-frame model P-frame g_a, h_a	Always hard quantization Finetune P-frame g_s, h_s

Table 1. The multi-stage quantization and training strategy. *AUN* refers to additive uniform noise [5]. *Hard* means hard quantization without gradient passing to encoder (encoder is fixed). Stage ④ and ⑤ can actually be merged into one stage.

first performs I-frame STH and then performs P-frame STH. The specific process is illustrated in Table 1. To better understand this multi-stage quantization and training strategy, we provide some discussions in Appendix B. This multi-stage quantization strategy improves the RD performance obviously as shown in the experimental section.

Modulated Loss

The modulated loss function assigns larger λ value for the later P frames. The goal of modulated loss is to balance the reconstruction quality of frames in one GoP unit, the concept of which has been implemented in [37, 42]. With its help, the later P frame will be reconstructed with better quality, mitigating temporal error propagation. We adopt this modulated loss when $T = 5$ (stage ④⑤⑥ in Table 1):

$$\mathcal{L} = \mathcal{R}_I + \lambda \cdot \mathcal{D}_I + \sum_{t=1}^{T-1} (\mathcal{R}_t + \mu_t \cdot \lambda \cdot \mathcal{D}_t). \quad (4)$$

The t -th P-frame is assigned with larger distortion constraint, controlled by a monotonously increasing coefficient μ_t . We set $\mu_1 = 1$ and $\mu_{t+1} - \mu_t = 0.2$ in our experiments.

4. Experiments

Datasets. Our efficient neural video codec (ENVC) is trained on Vimeo dataset [49], which contains 89,800 video clips with the resolution of 448×256 . Video frames are randomly cropped into 192×192 patches during training. We evaluate the performance of our proposed ENVC on multiple benchmark datasets including the UVG dataset [39], HEVC test sequences [43] and MCL-JCV [45]. The UVG dataset contains seven 1080p video sequences, with 3900 frames in total. The HEVC test sequences (Class B,C,D,E) contain videos with resolutions from 416×240 to 1920×1080 . The MCL-JCV dataset [45] is another common benchmark dataset which contains 30 video sequences in 1080p.

Implementation details. Section 3.4 introduces our training strategy. The specific learning rate and iteration number of each stage are added in Appendix B. Minibatch is always

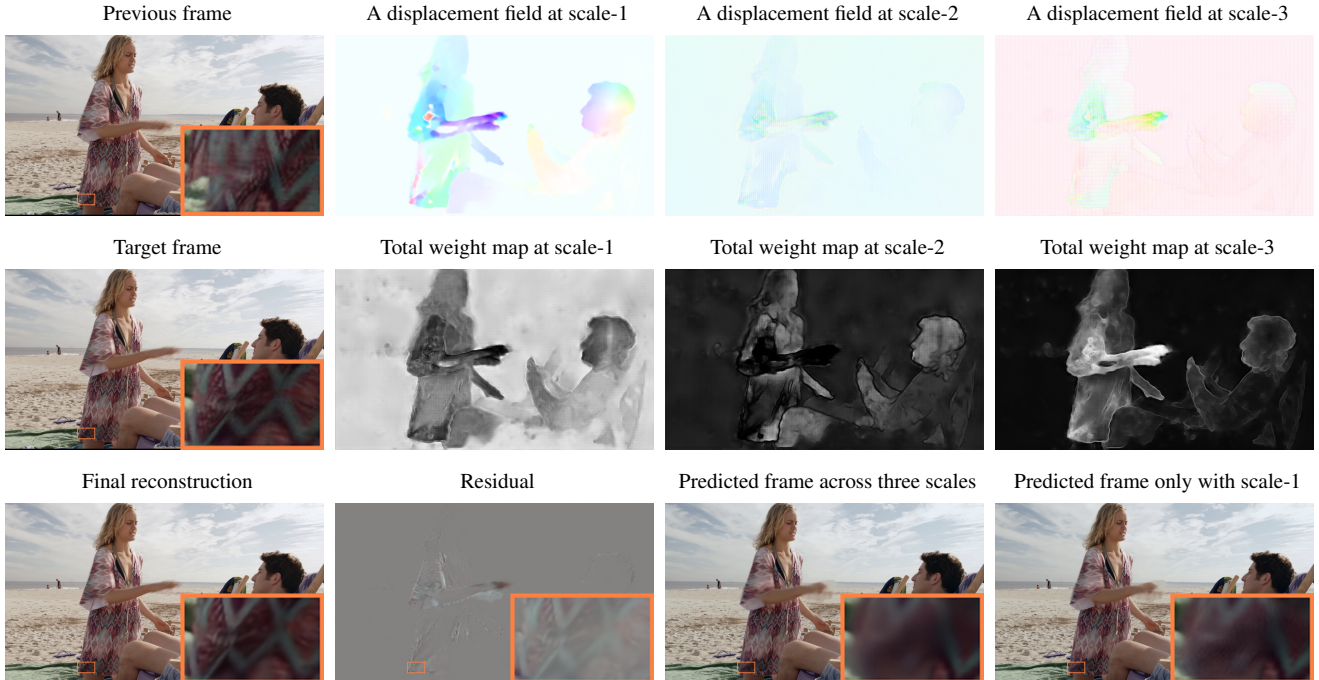


Figure 4. Visualizations of two consecutive frames, with corresponding cross-scale flows and cross-scale weight maps. Regarding the weight map, white color means the weight value is one and the black color means zero weight. It is found that prediction across scales can synthesize a fine prediction result which can better handle various motion cases. Noticeable noise can be found if predicting only with the high-resolution scale (scale-1). Zoom-in the last picture to check the unexpected prediction noise at scale-1.

set as 8 during training and we use Adam optimizer [24]. Training the complete ENVC requires 10 days. We use two NVIDIA 2080TI GPUs for the joint training stages.

Standard baselines and compared methods. For traditional standards, we compared with VTM-12.0 [44] and HM-16.21 [22] with exactly the same prediction mode, *i.e.*, prediction with the previous single reference frame as well as test GoP size of 12. See Appendix C for the specific coding configurations of standard anchors. Note that the videos are compressed in YUV444 format with these anchors. For neural video coding approaches, we only compare with three representative hybrid coding approaches DVC [35], SSF [2] and FVC [23]. The comparison with VTM is persuasive enough to demonstrate our state-of-the-art performance.

Other settings. We do not apply variable-rate technique and thereby train multiple models for various bitrates. We set $\lambda = \{512, 1024, 2048, 3072, 4096\}$ to optimize for MSE. When optimized for MS-SSIM [46], we set $\lambda = \{6, 14, 24, 36, 50\}$ and finetune from the MSE-optimized model. In addition, two versions of ENVC are optimized for MSE, with or without autoregressive (AR) context model. ENVC with AR delivers the optimal RD performance but simultaneously requires much more decoding time compared with ENVC w/o AR.

5. Performance and Analysis

5.1. Comparison on RD Performance

RD-curves. We compare the RD curve of ENVC with traditional and other ML-based codecs in Figure 5. The proposed ENVC with AR model achieves comparable RD performance with VTM-12.0 in the setting of single-reference prediction, which means for the first time, a neural video codec can compete with H.266/VVC regarding sRGB PSNR. When evaluated by MS-SSIM, which is a more perceptual-friendly metric, ENVC exceeds VTM-12.0 especially at high bitrates. We only provide the results of ENVC w/o AR when optimized for MS-SSIM, because our experiments find AR model brings only few gains with this metric. Since previous neural video codecs can barely compete with H.265/HEVC, our proposed ENVC outperforms DVC [35] and SSF [2] and FVC# [23] by a large margin. Note FVC# has been enhanced by multiple-reference prediction.

BD-rate savings. To quantitatively measure the RD performance of ENVC, we calculate the BD-rate savings [8] against VTM-12.0 in Table 2. Specifically, the performance of ENVC (with AR) exceeds VTM slightly on UVG dataset in terms of PSNR (about 3.04% BD-rate savings). Regarding MS-SSIM, ENVC (no AR version) achieves 9.12% savings on UVG dataset and 33.93% savings in Class D dataset.

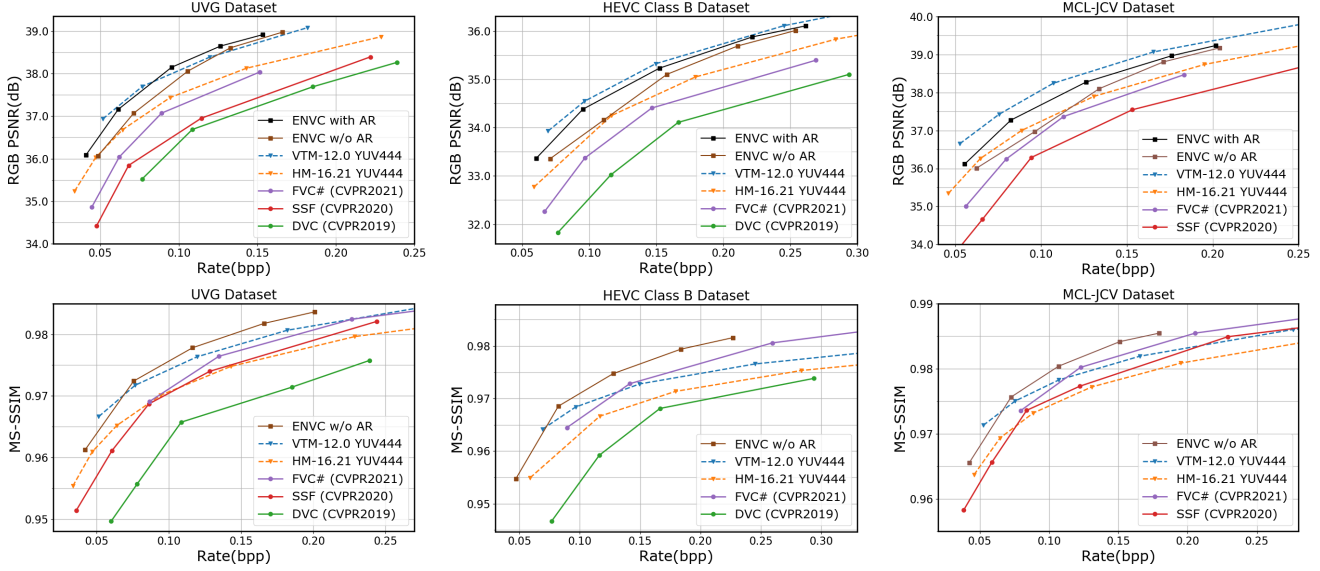


Figure 5. The RD-curve comparisons on UVG, HEVC Class B and MCL-JCV. We compare with previous neural video codecs according to the statistics reported in their papers. Note the performance of FVC# [23] is strengthened by a multiple-reference fusion module (marked by #), but still has a large gap with our ENVC.

Metric	Method	UVG 1920 × 1080	HEVC Class B 1920 × 1080	HEVC Class C 832 × 480	HEVC Class D 416 × 240	HEVC Class E 1280 × 720	MCL-JCV 1920 × 1080
PSNR	VTM-12.0	0%	0%	0%	0%	0%	0%
	ENVC with AR	- 3.04%	+ 6.95%	+ 34.74%	+ 16.00%	+ 16.11%	+ 15.50%
	ENVC w/o AR	+ 16.98%	+ 27.44%	+ 42.46%	+ 20.39%	+ 32.84%	+ 31.46%
	FVC#	+ 60.62%	+ 66.31%	+ 53.09%	+ 52.26%	Unknown	+ 53.97%
MS-SSIM	VTM-12.0	0%	0%	0%	0%	0%	0%
	ENVC w/o AR	- 9.12%	- 22.31%	- 17.07%	- 33.93%	- 20.34%	- 22.02%
	FVC#	+ 22.91%	+ 1.77%	- 3.64%	- 17.24%	Unknown	- 7.01%

Table 2. Calculating the BD-rate savings against VTM-12.0 on multiple benchmark datasets. + means more bits required. FVC# here is enhanced by multiple-reference prediction, but the performances of VTM and our ENVC are obtained only with single reference frame.

Compared with traditional codec VTM, it is interesting to find that neural video codecs can achieve higher PSNR in high-resolution datasets (such as UVG and Class B).

5.2. Analysis

Visualizations. As shown in Figure 4, we visualize both the cross-scale flows and weight maps. We remind our readers that although scales 1,2,3 correspond to $\frac{1}{2}$, $\frac{1}{4}$, $\frac{1}{8}$ original resolution, all the cross-scale flows and weight maps are at the scale of $\frac{H}{2} \times \frac{W}{2}$, the same as the scale of the predicted feature. There are multiple flows pointing to each scale (in our final model, $N=4$), and we only visualize the most important displacement field attending to each scale. It is observed that the displacement field at scale-1 is dense, which delivers a high-precision prediction. The displacement fields at scale-2 and scale-3 focus more on the region with complicated motion (such as the region of hand in Figure 4). Besides, we add all the weight maps at each scale, as the total weight map at scale-1,2,3. The visualizations of these weight maps

support our design motivation well. For example, in Figure 4, the weight map at scale-3 has larger weight value in the area including the lady’s hand and skirt edge, where the motion is complicated. Moreover, we can synthesize the predicted frame only with scale-1, by manually setting the weight values at scale-2 and scale-3 as zero. Now we can observe irregular noise in the zoom-in area of the last picture shown in Figure 4. It implies that high-resolution prediction will incur unexpected noise when motion is complicated. Prediction with low-resolution reference features can yield more compressible residuals in these areas. See more visualizations in Appendix E.

Cross-scale prediction v.s. other predictions. Our proposed cross-scale prediction supports fine-grained adaptation to diverse motion content. Here, we conduct an ablation study to compare the cross-scale prediction with other prediction approaches, including pixel-level [35], Gaussian-scale [2] and feature-level prediction [23]. The reproducing

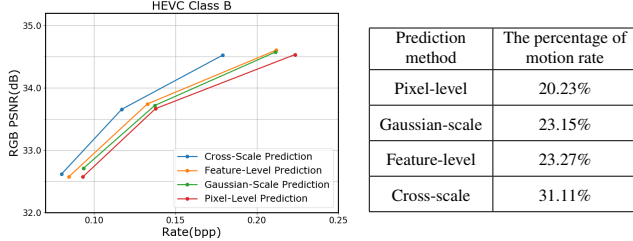


Figure 6. Left Figure: RD-curve comparison of different prediction methods. Right Table: The percentage of bits to encode motion information when $\lambda = 1024$. Here, pixel-level residual is directly computed without any motion compensation refinement network.

Component	GoP Structure for Training	Estimated Rate Savings
Base Model	I-P-P	0%
+ Feature Residual [17]	I-P-P	- 13%
More Training Frames & + Modulated Loss	I-P-P-P-P	- 18%
+ I-frame STH	I-P-P-P-P	- 20%
+ P-frame STH	I-P-P-P-P	- 27%
+ AR Model (ENVC with AR)	I-P-P-P-P	- 35%

Table 3. Ablation study on other important techniques. The base model is taken from Figure 6, which applies cross-scale prediction and computes the pixel-level residual.

settings are described in Appendix D. As shown in Figure 6, both Gaussian-scale prediction (SSF [2]) and feature-level prediction (FVC [23]) can increase the RD performance compared with the pixel-level prediction (DVC [35] without flow extractor). But our proposed cross-scale prediction brings another leap in RD performance, almost saving 20% rate compared with the conventional optical flow. In addition, we can observe an increase in the percentage of motion, since effective prediction consumes more bits on motion information but can reduce the rate of residuals.

Ablation on important techniques. We conduct a comprehensive experiment to demonstrate the effectiveness of every important component in our video codec. The model with cross-scale prediction and pixel-level residual shown in Figure 6 is taken as baseline. We gradually improve the RD performance by stacking techniques one by one. We calculate the BD-rate savings against the initial base mode, the results of which are presented in Table 3. It is found that feature-level residual [17] boosts performance obviously as it covers the gain of motion compensation refinement network [36]. More training frames ($T = 5$) and modulated loss bring a few gains (about 5%). Our proposed video-version soft-then-hard (I-frame STH + P-frame STH) achieves additional 9% savings (27-18=9%) without any complexity penalty during inference. The gain of AR model in video compression is not so obvious as in image compression [40]

Method	UVG (1080p)		HEVC Class C	
	Encoding(ms)	Decoding(ms)	Encoding(ms)	Decoding(ms)
ENVC with AR	711 (+2910)	433 (+34373)	142 (+510)	84 (+6984)
ENVC w/o AR	579 (+511)	337 (+567)	118 (+140)	70 (+165)
SSF +	487 (+651)	243 (+761)	100 (+203)	59 (+245)
DVC +	586 (+645)	350 (+753)	125 (+195)	74 (+225)

Table 4. Test the encoding/decoding time on RTX 2080Ti GPU. We report the average network inference time (+ practical arithmetic coding time) of P-frame. SSF [2] and DVC [35] are reproduced and enhanced by resblocks, marked as SSF+ and DVC+.

(only 35-27=8% savings here). This phenomenon can be explained because in hybrid video coding, most of the bits are spent for residual compression. Mask convolution is not well-suited to estimate the irregular context of residual.

About the scales. We finally choose three scales ($\frac{1}{2}, \frac{1}{4}, \frac{1}{8}$ resolution) for cross-scale prediction. On the one hand, features at scale $\frac{H}{16} \times \frac{W}{16}$ have lost much context information, which cannot bring more gains. On the other hand, producing reference features with higher spatial resolution (such as in pixel space or even sub-pixel space) consumes much more GPU memory. Feature at scale $\frac{H}{2} \times \frac{W}{2}$ preserves enough context to deliver a high-precision prediction.

5.3. Complexity

Our I-frame compression model contains 12.23 M parameters and our P-frame compression model contains 21.07 M parameters. To evaluate the time complexity, we study on two datasets with different resolutions. The network inference time is shown in Table 4, independent with the time of arithmetic coding which is very sensitive to practical implementations. It is found that the network inference time of ENVC w/o AR is between the enhanced SSF [2] and DVC [35]. Because on the one hand, DVC is an early framework containing an explicit optical flow extractor. On the other hand, our proposed cross-scale prediction module relies on bilinear sampling, which can be computed very fast and thereby does not increase the coding time obviously. In addition, ENVC with AR model requires much more coding time, mainly spent for arithmetic coding, especially arithmetic decoding.

6. Conclusion

In this paper, we present an efficient neural video codec (ENVC) with a novel cross-scale prediction module. The proposed cross-scale prediction module achieves more effective motion compensation result through fine-grained adaptation to diverse motion cases. Cross-scale flows are transmitted to control the prediction precisions with a reference feature pyramid. We also propose to transmit cross-scale weight maps to compute the result of weighted prediction. We carefully build the model and adopt a new multi-stage quantization strategy. ENVC is the first neural video codec that

can compete with VTM regarding sRGB PSNR under the configuration of single-reference prediction, which opens up a new gate for neural video compression. It can further be extended to other prediction configurations in future work.

References

- [1] Eirikur Agustsson, Fabian Mentzer, Michael Tschannen, Lukas Cavigelli, Radu Timofte, Luca Benini, and Luc V Gool. Soft-to-hard vector quantization for end-to-end learning compressible representations. In *Advances in Neural Information Processing Systems 30*, pages 1141–1151, 2017. [2](#)
- [2] Eirikur Agustsson, David Minnen, Nick Johnston, Johannes Balle, Sung Jin Hwang, and George Toderici. Scale-space flow for end-to-end optimized video compression. In *Proceedings of the IEEE/CVF Conference on Computer Vision and Pattern Recognition*, pages 8503–8512, 2020. [1](#), [3](#), [6](#), [7](#), [8](#), [12](#), [13](#)
- [3] Eirikur Agustsson and Lucas Theis. Universally quantized neural compression. In *Advances in Neural Information Processing Systems*, volume 33, pages 12367–12376, 2020. [2](#), [5](#)
- [4] Eirikur Agustsson, Michael Tschannen, Fabian Mentzer, Radu Timofte, and Luc Van Gool. Generative adversarial networks for extreme learned image compression. In *Proceedings of the IEEE/CVF International Conference on Computer Vision*, pages 221–231, 2019. [2](#)
- [5] Johannes Ballé, Valero Laparra, and Eero P. Simoncelli. End-to-end optimized image compression. In *5th International Conference on Learning Representations, ICLR 2017*, 2017. [2](#), [3](#), [5](#), [11](#)
- [6] Johannes Ballé, David Minnen, Saurabh Singh, Sung Jin Hwang, and Nick Johnston. Variational image compression with a scale hyperprior. In *6th International Conference on Learning Representations, ICLR 2018*, 2018. [1](#), [2](#), [11](#)
- [7] Yoshua Bengio, Nicholas Léonard, and Aaron Courville. Estimating or propagating gradients through stochastic neurons for conditional computation. *arXiv preprint arXiv:1308.3432*, 2013. [5](#), [12](#)
- [8] Gisle Bjontegaard. Calculation of average psnr differences between rd-curves. *VCEG-M33*, 2001. [6](#)
- [9] Benjamin Bross, Ye-Kui Wang, Yan Ye, Shan Liu, Jianle Chen, Gary J. Sullivan, and Jens-Rainer Ohm. Overview of the versatile video coding (vvc) standard and its applications. *IEEE Transactions on Circuits and Systems for Video Technology*, 31(10):3736–3764, 2021. [1](#), [2](#), [3](#)
- [10] Zhibo Chen, Tianyu He, Xin Jin, and Feng Wu. Learning for video compression. *IEEE Transactions on Circuits and Systems for Video Technology*, 30(2):566–576, 2019. [1](#), [3](#)
- [11] Zhengxue Cheng, Heming Sun, Masaru Takeuchi, and Jiro Katto. Learned image compression with discretized gaussian mixture likelihoods and attention modules. In *Proceedings of the IEEE/CVF Conference on Computer Vision and Pattern Recognition*, pages 7939–7948, 2020. [1](#), [2](#)
- [12] Yoojin Choi, Mostafa El-Khamy, and Jungwon Lee. Variable rate deep image compression with a conditional autoencoder. In *Proceedings of the IEEE International Conference on Computer Vision*, pages 3146–3154, 2019. [2](#)
- [13] Ze Cui, Jing Wang, Shangyin Gao, Tiansheng Guo, Yihui Feng, and Bo Bai. Asymmetric gained deep image compression with continuous rate adaptation. In *Proceedings of the IEEE/CVF Conference on Computer Vision and Pattern Recognition*, pages 10532–10541, 2021. [2](#)
- [14] Jifeng Dai, Haozhi Qi, Yuwen Xiong, Yi Li, Guodong Zhang, Han Hu, and Yichen Wei. Deformable convolutional networks. In *Proceedings of the IEEE international conference on computer vision*, pages 764–773, 2017. [4](#)
- [15] Abdelaziz Djelouah, Joaquim Campos, Simone Schaub-Meyer, and Christopher Schroers. Neural inter-frame compression for video coding. In *Proceedings of the IEEE/CVF International Conference on Computer Vision*, pages 6421–6429, 2019. [1](#), [2](#), [3](#)
- [16] Runsen Feng, Zongyu Guo, Zhizheng Zhang, and Zhibo Chen. Versatile learned video compression. *arXiv preprint arXiv:2111.03386*, 2021. [3](#)
- [17] Runsen Feng, Yaojun Wu, Zongyu Guo, Zhizheng Zhang, and Zhibo Chen. Learned video compression with feature-level residuals. In *Proceedings of the IEEE/CVF Conference on Computer Vision and Pattern Recognition Workshops*, pages 120–121, 2020. [3](#), [4](#), [8](#), [13](#)
- [18] Zongyu Guo, Zhizheng Zhang, Runsen Feng, and Zhibo Chen. Causal contextual prediction for learned image compression. *IEEE Transactions on Circuits and Systems for Video Technology*, pages 1–1, 2021. [1](#), [2](#)
- [19] Zongyu Guo, Zhizheng Zhang, Runsen Feng, and Zhibo Chen. Soft then hard: Rethinking the quantization in neural image compression. In *Proceedings of the 38th International Conference on Machine Learning*, volume 139, pages 3920–3929. PMLR, 2021. [2](#), [5](#), [11](#)
- [20] Ali Habibi. Hybrid coding of pictorial data. *IEEE Transactions on Communications*, 22(5):614–624, 1974. [1](#), [3](#)
- [21] Amirhossein Habibian, Ties van Rozendaal, Jakub M Tomczak, and Taco S Cohen. Video compression with rate-distortion autoencoders. In *Proceedings of the IEEE/CVF International Conference on Computer Vision*, pages 7033–7042, 2019. [1](#), [3](#)
- [22] HM. Hvc official test model. <https://hevc.hhi.fraunhofer.de>, 2021. [6](#)
- [23] Zhihao Hu, Guo Lu, and Dong Xu. Fvc: A new framework towards deep video compression in feature space. In *Proceedings of the IEEE/CVF Conference on Computer Vision and Pattern Recognition*, pages 1502–1511, 2021. [1](#), [3](#), [4](#), [6](#), [7](#), [8](#), [13](#)
- [24] Diederik P Kingma and Jimmy Ba. Adam: A method for stochastic optimization. *arXiv preprint arXiv:1412.6980*, 2014. [6](#)
- [25] Théo Ladune, Pierrick Philippe, Wassim Hamidouche, Lu Zhang, and Olivier Déforges. Conditional coding for flexible learned video compression. In *International Conference on Learning Representations (ICLR) 2021, Neural Compression Workshop*, 2021. [2](#), [3](#)
- [26] Jooyoung Lee, Seunghyun Cho, and Seung-Kwon Beack. Context-adaptive entropy model for end-to-end optimized image compression. In *7th International Conference on Learning Representations, ICLR 2019*, 2019. [2](#)

- [27] Jiahao Li, Bin Li, and Yan Lu. Deep contextual video compression. *arXiv preprint arXiv:2109.15047*, 2021. **3**
- [28] Jianping Lin, Dong Liu, Houqiang Li, and Feng Wu. M-lvc: multiple frames prediction for learned video compression. In *Proceedings of the IEEE/CVF Conference on Computer Vision and Pattern Recognition*, pages 3546–3554, 2020. **1, 3**
- [29] Tsung-Yi Lin, Piotr Dollár, Ross Girshick, Kaiming He, Bharath Hariharan, and Serge Belongie. Feature pyramid networks for object detection. In *Proceedings of the IEEE conference on computer vision and pattern recognition*, pages 2117–2125, 2017. **2, 4**
- [30] Tony Lindeberg. *Scale-space theory in computer vision*, volume 256. Springer Science & Business Media, 2013. **1**
- [31] Haojie Liu, Ming Lu, Zhan Ma, Fan Wang, Zhihuang Xie, Xun Cao, and Yao Wang. Neural video coding using multi-scale motion compensation and spatiotemporal context model. *IEEE Transactions on Circuits and Systems for Video Technology*, 31(8):3182–3196, 2021. **1, 3, 4**
- [32] Jerry Liu, Shenlong Wang, Wei-Chiu Ma, Meet Shah, Rui Hu, Pranaab Dhawan, and Raquel Urtasun. Conditional entropy coding for efficient video compression. In *Computer Vision—ECCV 2020: 16th European Conference, Glasgow, UK, August 23–28, 2020, Proceedings, Part XVII 16*, pages 453–468. Springer, 2020. **1, 3**
- [33] Ze Liu, Yutong Lin, Yue Cao, Han Hu, Yixuan Wei, Zheng Zhang, Stephen Lin, and Baining Guo. Swin transformer: Hierarchical vision transformer using shifted windows. In *Proceedings of the IEEE/CVF International Conference on Computer Vision (ICCV)*, pages 10012–10022, October 2021. **2**
- [34] Guo Lu, Chunlei Cai, Xiaoyun Zhang, Li Chen, Wanli Ouyang, Dong Xu, and Zhiyong Gao. Content adaptive and error propagation aware deep video compression. In *European Conference on Computer Vision*, pages 456–472. Springer, 2020. **3**
- [35] Guo Lu, Wanli Ouyang, Dong Xu, Xiaoyun Zhang, Chunlei Cai, and Zhiyong Gao. Dvc: An end-to-end deep video compression framework. In *Proceedings of the IEEE/CVF Conference on Computer Vision and Pattern Recognition*, pages 11006–11015, 2019. **1, 3, 6, 7, 8, 13**
- [36] Guo Lu, Xiaoyun Zhang, Wanli Ouyang, Li Chen, Zhiyong Gao, and Dong Xu. An end-to-end learning framework for video compression. *IEEE transactions on pattern analysis and machine intelligence*, 2020. **8, 13**
- [37] Fabian Mentzer, Eirikur Agustsson, Johannes Ballé, David Minnen, Nick Johnston, and George Toderici. Towards generative video compression. *arXiv preprint arXiv:2107.12038*, 2021. **5**
- [38] Fabian Mentzer, George D Toderici, Michael Tschannen, and Eirikur Agustsson. High-fidelity generative image compression. In *Advances in Neural Information Processing Systems*, volume 33, pages 11913–11924, 2020. **1, 2**
- [39] Alexandre Mercat, Marko Viitanen, and Jarno Vanne. Uvg dataset: 50/120fps 4k sequences for video codec analysis and development. In *Proceedings of the 11th ACM Multimedia Systems Conference*, pages 297–302, 2020. **2, 5**
- [40] David Minnen, Johannes Ballé, and George Toderici. Joint autoregressive and hierarchical priors for learned image compression. In *Advances in Neural Information Processing Systems 31*, pages 10771–10780, 2018. **2, 8, 11**
- [41] Reza Pourreza and Taco Cohen. Extending neural p-frame codecs for b-frame coding. In *Proceedings of the IEEE/CVF International Conference on Computer Vision (ICCV)*, pages 6680–6689, October 2021. **1, 3**
- [42] Oren Rippel, Alexander G Anderson, Kedar Tatwawadi, Sanjay Nair, Craig Lytle, and Lubomir Bourdev. Elf-vc: Efficient learned flexible-rate video coding. *arXiv preprint arXiv:2104.14335*, 2021. **1, 3, 5**
- [43] Gary J Sullivan, Jens-Rainer Ohm, Woo-Jin Han, and Thomas Wiegand. Overview of the high efficiency video coding (hevc) standard. *IEEE Transactions on Circuits and Systems for Video Technology*, 22(12):1649–1668, 2012. **1, 2, 3, 5**
- [44] VTM. Vvc official test model. <https://jvet.hhi.fraunhofer.de>, 2021. **6**
- [45] Haiqiang Wang, Weihao Gan, Sudeng Hu, Joe Yuchieh Lin, Lina Jin, Longguang Song, Ping Wang, Ioannis Katsavounidis, Anne Aaron, and C-C Jay Kuo. Mcl-jcv: a jnd-based h. 264/avc video quality assessment dataset. In *2016 IEEE International Conference on Image Processing (ICIP)*, pages 1509–1513. IEEE, 2016. **2, 5**
- [46] Zhou Wang, Alan C Bovik, Hamid R Sheikh, and Eero P Simoncelli. Image quality assessment: from error visibility to structural similarity. *IEEE transactions on image processing*, 13(4):600–612, 2004. **2, 6**
- [47] Thomas Wiegand, Gary J Sullivan, Gisle Bjontegaard, and Ajay Luthra. Overview of the h. 264/avc video coding standard. *IEEE Transactions on circuits and systems for video technology*, 13(7):560–576, 2003. **1, 3**
- [48] Chao-Yuan Wu, Nayan Singhal, and Philipp Krahenbuhl. Video compression through image interpolation. In *Proceedings of the European Conference on Computer Vision (ECCV)*, pages 416–431, 2018. **1, 3**
- [49] Tianfan Xue, Baian Chen, Jiajun Wu, Donglai Wei, and William T Freeman. Video enhancement with task-oriented flow. *International Journal of Computer Vision*, 127(8):1106–1125, 2019. **5**
- [50] Ren Yang, Fabian Mentzer, Luc Van Gool, and Radu Timofte. Learning for video compression with hierarchical quality and recurrent enhancement. In *Proceedings of the IEEE/CVF Conference on Computer Vision and Pattern Recognition*, pages 6628–6637, 2020. **1, 3**
- [51] Yibo Yang, Robert Bamler, and Stephan Mandt. Improving inference for neural image compression. In *Advances in Neural Information Processing Systems*, volume 33, pages 573–584, 2020. **2**
- [52] Xizhou Zhu, Han Hu, Stephen Lin, and Jifeng Dai. Deformable convnets v2: More deformable, better results. In *Proceedings of the IEEE/CVF Conference on Computer Vision and Pattern Recognition*, pages 9308–9316, 2019. **4**
- [53] Xizhou Zhu, Weijie Su, Lewei Lu, Bin Li, Xiaogang Wang, and Jifeng Dai. Deformable detr: Deformable transformers for end-to-end object detection. In *International Conference on Learning Representations*, 2020. **2, 4**

Appendix A: Network Structures

All the enhancement modules used in our model are resblocks. We here explain how these resblocks are built. As shown in Figure 7a, one resblock refers to a residual connection with two convolutional layers. We stack three successive resblocks as one unit to enhance the network, which is termed as resblocks as shown in Figure 7b. The structures of the autoencoder used for I-frame compression are described in Figure 7c. We can observe that every down/up-sampling layer is followed by the unit of resblocks. Note that there are four downsampling layers in I-frame encoder. However, since we apply cross-scale feature prediction and compute the feature-level residual, there are only three downsampling layers in both the motion and the residual encoders. In addition, the structures of the multi-scale feature extractor are described in Figure 7d, where two downsampling layers with resblocks will transform the original reference feature from the scale of $\frac{H}{2} \times \frac{W}{2}$ to the scale of $\frac{H}{4} \times \frac{W}{4}$ and $\frac{H}{8} \times \frac{W}{8}$.

Following most previous works, we control the network capacity with two hyper parameters N and M . In the I-frame compression network, we set $N = 128$ and $M = 160$. In the motion compression network, we set $N = 64$ and $M = 80$ because the rate of motion is relatively small. In the residual compression network, we set $N = 128$ and $M = 160$.

Regarding the entropy model, we use three kinds of entropy model, including the conventional factorized model [5] and hyperprior entropy model [6] and the autoregressive entropy model [40]. For ENVC w/o AR, we apply hyperprior model for I-frame compression and residual compression. Factorized model is applied for motion compression. For ENVC with AR, we apply autoregressive entropy model in all three compression networks. However, the entropy model in our motion compression network does not contain a hyperprior branch. That is to say, we directly use mask convolution and parameterize the motion variables as GMM distribution. We find this kind of AR model is stable and more effective for motion compression, because the context of motion information is very smooth.

Appendix B: Video Soft-Then-Hard

Quantization is one of the core techniques for lossy data compression. Most prevailing image compression methods apply additive uniform noise (AUN) [5] during training to approximate the test-time rounding operation. However, AUN will incur a train-test mismatch issue, which would lead to an obvious rate point shift. In particular, the rate estimated during training (differential entropy) has a gap to what we want to minimize for testing (discrete entropy). One previous work [19] proposes a simple yet effective approach, *i.e.*, soft-then-hard (STH), to close the train-test mismatch of image compression model. The image-version STH suggests fixing the encoder and hyper encoder, and tuning the decoder

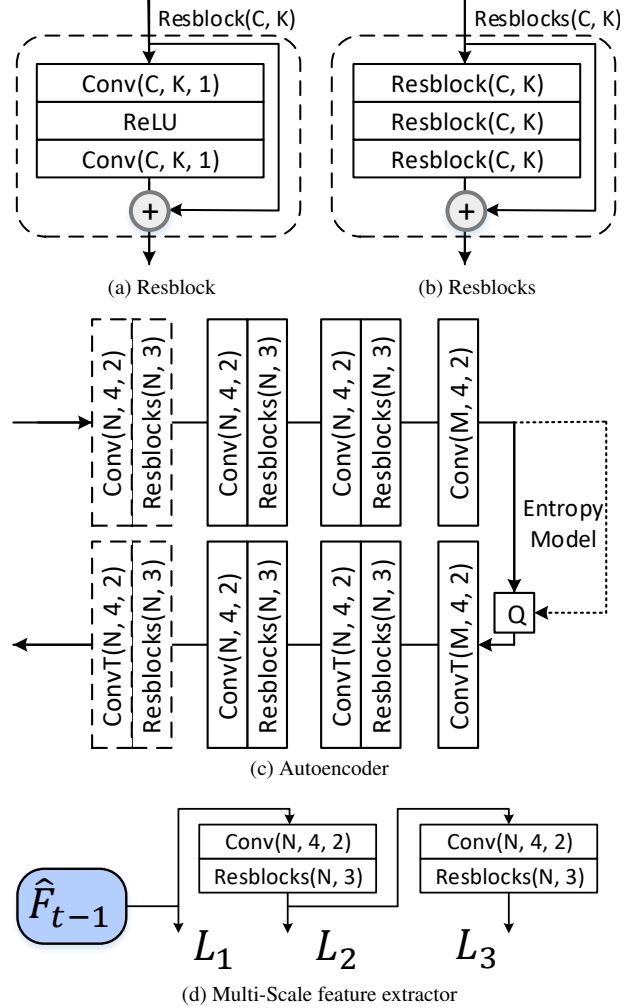


Figure 7. Specific network structures.

and hyper decoder without gradient passing to the encoder. And the decoder and hyper decoder are fed with the hard-quantized latent variables and can be optimized with the true rate-distortion value. However, for video compression, since the P-frame model is recurrently used, the gradient needs to pass through the P-frame encoders. Therefore, the image-version STH cannot be directly applied.

In this paper, we propose a multi-stage quantization strategy, as the video-version STH, to gradually close the train-test mismatch of AUN. Specifically, we first apply AUN to optimize I-frame model and P-frame model together, then adopt I-frame STH and P-frame STH, respectively. In our main paper, we have listed our training strategy as six stages. You can look back on the Table 1 in our main paper.

B1: I-Frame Soft-Then-Hard

The I-frame STH can easily be adopted. After jointly optimizing the P-frame model and the I-frame model with

training GoP size $T = 3$, we increase T to 5 and adopt the I-frame STH simultaneously. Specifically, we now fix the I-frame encoder and hyper encoder, and jointly optimize the I-frame decoder and hyper decoder with the entire P-frame model. As shown in Figure 8a, we directly quantize the I-frame latent variables by hard rounding, and the quantization in P-frame model is still approximated by AUN. Note that in Figure 8a, we do not visualize the entropy model including the hyper encoder and hyper decoder.

The I-frame STH has two advantages. First of all, it is obvious that the I-frame model will not suffer from the train-test mismatch issue of AUN-based quantization any more since the I-frame encoder and hyper encoder are fixed. Therefore, the performance of I-frame compression can be increased obviously, *i.e.*, smaller rate and lower distortion. In addition, the I-frame STH assists to keep the rate of I-frame balanced with the rate of P-frame. We note that the I-frame rate occupies most of the rate in a GoP unit. If directly optimizing an I-frame with many P-frames, it would make the entire codec pay much attention to I-frame rate and fails to train a good P-frame model. Some previous works take a trivial solution that prevents the gradient passing from I-frame model to P-frame model [2]. But such an optimization strategy makes the I-frame reconstruction result unsuitable for predicting the next P-frame. The I-frame STH used here can build an I-frame decoder that produces an I-frame reconstruction well-suited for P-frame prediction.

B2: P-Frame Soft-Then-Hard

Our P-frame compression model mainly contains a motion compression network and a residual compression network. To close the train-test mismatch of AUN in these two sub-networks, we further apply the two-stage P-frame soft-then-hard strategy. As shown in Figure 8b, after adopting the I-frame STH to finetune the codec, we will fix the I-frame model and the motion encoder in P-frame model. However, different from the original STH, here the later P-frames need to pass gradient through the motion encoder, so we apply straight-through estimator (STE) [7] for gradient passing. And the motion rate is estimated as an independent discrete density estimation model. Now we could solve the train-test mismatch caused by the AUN-based quantization for motion compression.

To further close the train-test mismatch of quantization for residual compression, we finally fix all the components except the residual decoder and hyper decoder. Now the gradient will not pass into any encoder, as shown in Figure 8c. The residual decoder and hyper decoder are directly optimized with the hard-quantized variables.

As the ablation experiment shown in our main paper, the I-frame STH brings about 2% rate savings and the P-frame STH brings additional 7% rate savings.

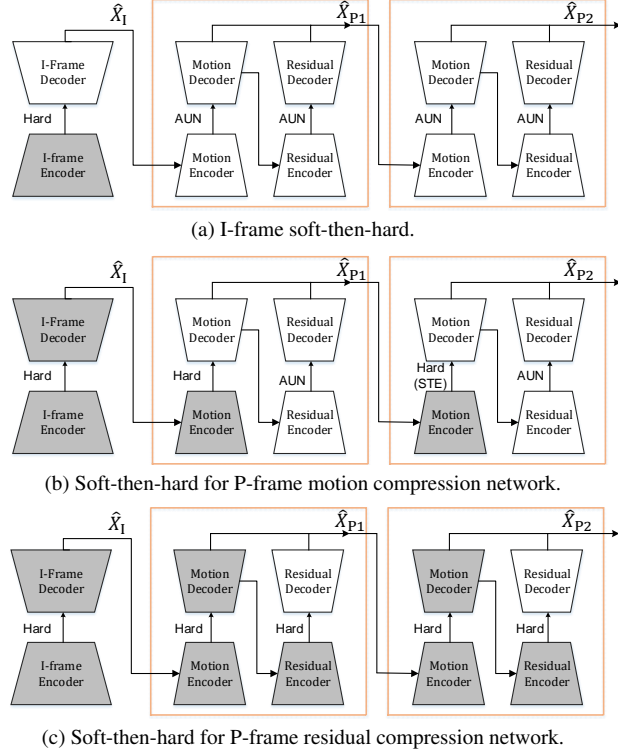


Figure 8. Video-version soft-then-hard. The gray box here means the corresponding module is fixed at this stage. *Hard* refers to hard quantization. *Hard(STE)* refers to hard quantization and gradient passing with straight-through estimator (STE) [7].

B3: Training Details

We use the Adam optimizer as illustrated in our main paper. The I-frame model and the P-frame model are pre-trained independently for 1 million iterations with learning rate of $5e-5$. Then the entire model is optimized with training GoP size $T = 3$. This stage takes 200,000 iterations, where the learning rate decays to $1e-5$ after 100,000 iterations. The training GoP size T is then increased to 5 and we adopt the modulated loss together. Actually, we also apply the I-frame STH as soon as we increase T , *i.e.*, stage ④ and ⑤ in Table 1 in the main paper are integrated into one training stage. This stage lasts for 50,000 iterations, where the learning rate decay from $5e-5$ to $1e-5$ after 20,000 iterations. The P-frame STH stage (for either motion compression or residual compression) takes a short period for finetuning, as 20,000 iterations with a learning rate of $1e-5$.

Appendix C: Configurations of HM and VTM

All the source test videos are in YUV420 format, which is also the default input format of HM and VTM. However, existing learning-based methods are optimized and evaluated in RGB color space. To make a fair comparison, we

first convert the test videos to RGB images as the input of learning-based codecs, and then convert them back into YUV444 format as the input of the traditional codecs. All codecs are finally evaluated in RGB color space. The detailed coding configurations are described as follows.

HM-16.21 We use the default configuration file “encoder_lowdelay_P_main.cfg” of HM-16.21 and encode the test videos with the following command:

```
TAppEncoderStatic -c [CFG] -i [IN].yuv -b [OUT].bin
-o [OUT].yuv -wdt [W] -hgt [H] -fr [FPS] -f [N]
-q [QP] --IntraPeriod=12 --Profile=main_444
--InputChromaFormat=444 --Level=6.1
--ConformanceWindowMode=1
```

Here, N is the number of encoded frames, which is set as 100 for HEVC datasets and 600 for UVG dataset.

VTM-12.0 We use the default configuration file “encoder_lowdelay_P_vtm.cfg” of VTM-12.0 and modified the GoP structure to fit the keyframe (I-frame) interval of 12, as shown in Table 5. We encode the test videos with the following command:

```
EncoderAppStatic -c [CFG] -i [IN].yuv -b [OUT].bin
-o [OUT].yuv -wdt [W] -hgt [H] -fr [FPS] -f [N]
-q [QP] --IntraPeriod=12 -c yuv444.cfg
--InputBitDepth=8 --OutputBitDepth=8
--InputChromaFormat=444 --Level=6.1
--DecodingRefreshType=2
--ConformanceWindowMode=1
```

Here, N is the number of encoded frames, which is set as 100 for HEVC datasets and 600 for UVG dataset.

Appendix D: Specific Settings for Ablation

In our main paper, we present an ablation experiment to investigate the performance of different prediction methods, including pixel-level prediction [35], Gaussian-scale prediction [2], feature-level prediction [23] and our proposed cross-scale prediction. Here we add some details about our ablation settings.

We compute the conventional pixel-level residual for all the four prediction methods, since pixel-level and Gaussian-scale prediction are performed in original pixel domain. However, the feature-level prediction and our proposed cross-scale prediction generate predicted features which are at the scale of $\frac{1}{2}$ original resolution. Therefore, for the latter two prediction approaches, we apply an additional upsampling convolutional layer after prediction and then compress the

pixel-level residual. Note that no motion compensation refinement network is applied for all the four prediction approaches in this ablation study. We also highlight that the feature-level prediction and the proposed cross-scale prediction are more applicable to be combined with feature-level residual [17].

We emphasize that since the autoencoders used for motion compression and residual compression have been enhanced by many residual blocks, the pixel-level prediction with pixel-level residual can already achieve good performance, similar to the result in DVC.Pro [36]. That is why pixel-level prediction and Gaussian-level prediction in our ablation study present a small gap in rate-distortion performance. Even though the baseline model is powerful enough, our proposed cross-scale prediction further boosts the rate-distortion performance. Therefore, this ablation study verifies the effectiveness of the cross-scale prediction solidly.

Appendix E: More Visualizations

E1: Visual Comparisons with VTM

The ENVC proposed in this paper can compete with VTM in terms of sRGB PSNR on UVG dataset. And it further outperforms VTM in terms of MS-SSIM quantitatively. We here provide some visual comparisons with VTM, as shown in Figure 9. The reconstruction results of ENVC present better perceptual quality especially when optimized by MS-SSIM. In HEVC Class B dataset, where videos has more complicated motion, our ENVC with cross-scale prediction presents satisfactory reconstruction quality.

E2: Visualizations of Cross-Scale Prediction

It is important to visualize the cross-scale flows and the cross-scale weight maps. Here we provide more examples that demonstrate the content-adaptive characteristics of the cross-scale prediction, as shown in Figure 10.

We also want to add some details about how we generate the visualizations. If the original image resolution is $H \times W$, we produce a reference feature pyramid at the scale of $\frac{1}{2}, \frac{1}{4}, \frac{1}{8}$ resolution. The predicted feature is at the scale of $\frac{H}{2} \times \frac{W}{2}$. The scale of displacement vectors and weight maps are exactly the same as the scale of the predicted feature, since every spatial location in the predicted feature requires corresponding displacement vectors and weight maps. In order to visualize the predicted frame shown in our main paper, which is at the original image scale, we directly produce the final reconstruction by setting the feature residual as zero.

As shown here in Figure 10, it is obvious that the cross-scale prediction relies on high-resolution reference feature for prediction in these areas with simple motion. But for these areas with fast motion or complicated motion, the low-resolution scale is of great significance since the weight value assigned to scale-3 is large in these fast-motion areas.

	Type	POC	QPOffset	QPOffsetModelOff	QPOffsetModelScale	#ref_pics_L0	reference_pictures_L0
Frame1	P	1	5	-6.5	0.2590	4	1 7 13 19
Frame2	P	2	4	-6.5	0.2590	4	1 2 8 14
Frame3	P	3	5	-6.5	0.2590	4	1 3 9 15
Frame4	P	4	4	-6.5	0.2590	4	1 4 10 16
Frame5	P	5	5	-6.5	0.2590	4	1 5 11 17
Frame6	P	6	1	0	0.0	4	1 6 12 18

Table 5. We modify the GoP structure of VTM-12.0, in order to keep the test conditional always with GoP size as 12.

E3: Multi-Head Warping

In our final model, we apply multi-head warping (prediction) that separates the reference feature pyramid into four channel groups. In each group, we perform the cross-scale warping independently. Among the four channel groups, we find two of these channel groups have primary effects on the warping results. Figure 11 visualizes the weight maps in these two channel groups. We experimentally find that this multi-head warping operator helps to accelerate and stabilize the training process, although achieves similar rate-distortion performance as single-head warping.



(a) Ground Truth



(b) VTM-12.0
0.0449bpp / 35.38dB / 0.9596 MS-SSIM



(c) ENVC with AR, optimized for MSE
0.0400bpp / 35.42dB / 0.9599



(d) ENVC w/o AR, optimized for MS-SSIM
0.0605bpp / 33.61dB / **0.9621**

Figure 9. Visual Comparison with VTM-12.0.



Figure 10. Visualizations of cross-scale flows and cross-scale weight maps. Scale-1,2,3 refer to 1/2, 1/4, 1/8 original spatial resolution. The areas with fast motion will be predicted with larger weight value assigned to scale-3. For the weight map, white color means the weight value is close to 1 and the black color means the weight value is close to 0.

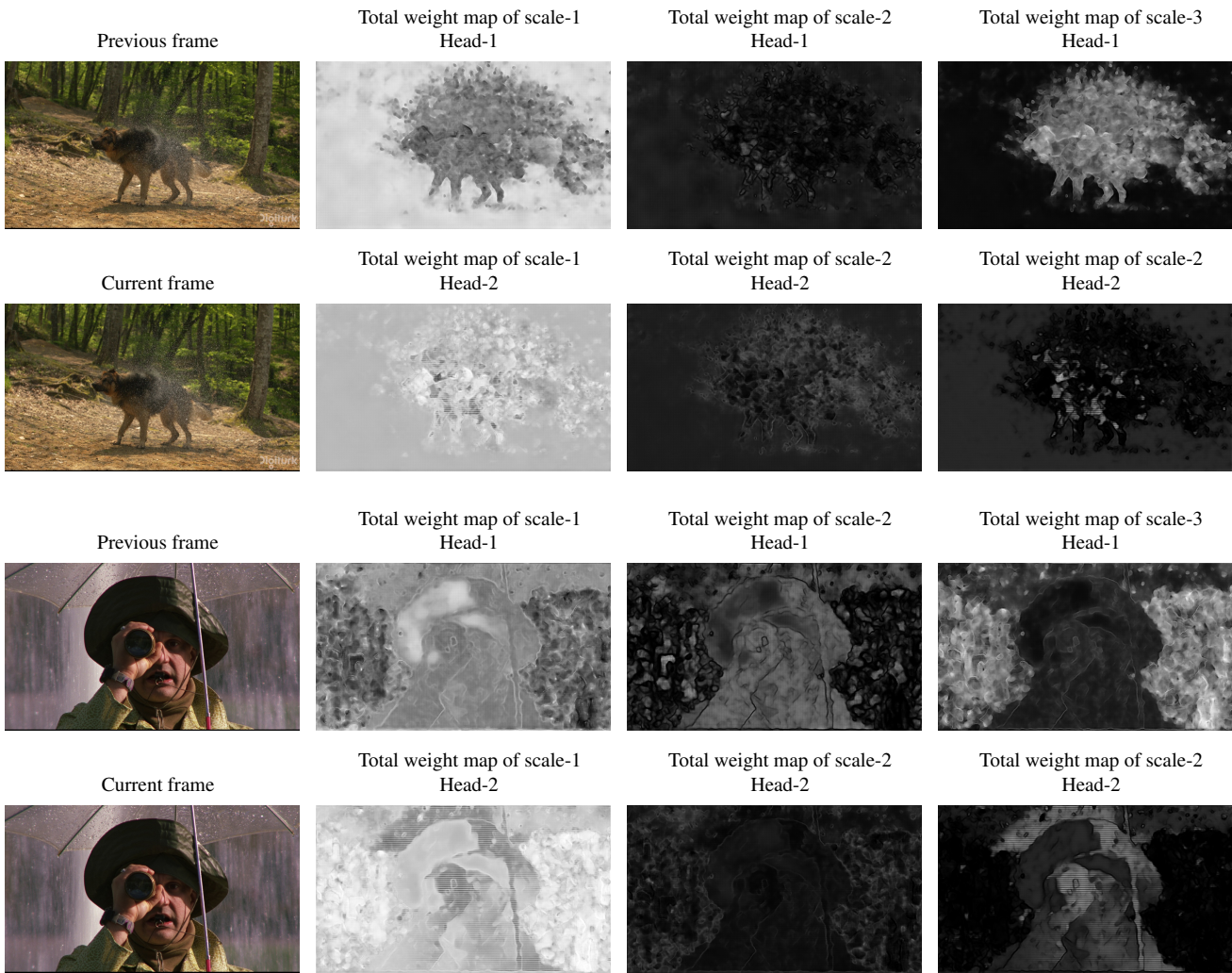


Figure 11. Visualization of multi-head warping. Two heads have primary effects to the final prediction result.